nature communications



Article

https://doi.org/10.1038/s41467-025-65214-z

$SL(2, \mathbb{C})$ non-Abelian gauge fields in a photonic molecule array

Received: 1 April 2025

Accepted: 10 October 2025

Published online: 19 November 2025

Check for updates

Zhaohui Dong ¹, Xianfeng Chen ^{1,2,3} & Luqi Yuan ¹∠

Engineering the topological properties of the system has been a longstanding subject in physics. Here, we propose a scheme to simulate topological materials with a non-Abelian gauge field in synthetic space-frequency dimensions where the symmetry between spin-flipped hoppings can be levitated by using coupled photonic molecules under dynamic modulations. The frequency-split supermodes in these photonic molecules can serve the pseudospin degree of freedom, which can further be connected along the frequency axis in an independent way, offering the unique opportunity to explore topological physics with imbalanced spin-flipped hoppings leading to a complex generalization of the conventional SU(2) non-Abelian gauge field, i.e., an SL(2, C) gauge field. By varying the spin-flipped hopping terms, we theoretically show the existence of a variety of Dirac semimetal transitions and the rotation of the pseudospin projection for the edge states throughout the Brillouin zone. Our proposal is experimentally feasible and therefore provides a versatile platform for the study of topological materials under non-Abelian gauge fields in photonics.

Exploring and controlling novel phases of matter has been a prominent subject in physics. Apart from variation of an external parameter such as temperature, pressure, or magnetic field, a synthetic gauge field has been proven to be a powerful tool in constructing and manipulating novel phases of matter, especially for neutral particle¹⁻³. In particular, the non-Abelian gauge field⁴⁻⁹, manifest in a wide range of distinct fields in physics such as high-energy physics, condensed-matter physics and electromagnetism, offering an effective way to synthesize exotic topological phases¹⁰⁻²⁰. Such a kind of gauge field is associated with the concept of the non-Abelian group in mathematics, as they hold non-commutative (non-Abelian) matrix-form components, which provides a framework for describing the statistics of spinful particles.

It has been growing interest in synthesizing non-Abelian gauge fields in diverse platforms. Compared to continuum systems^{21–26}, a non-Abelian gauge field in a lattice model has only been demonstrated in a few platforms, such as ultracold atoms^{27–30}, electrical circuits^{31,32} and photonic systems³³. However, these works focus on the realization of an SU(2) gauge field, while a non-Abelian gauge field does not

necessarily belong to the SU(2) group. For example, the complex generalization of the SU(2) group [i.e., the SL(2, \mathbb{C}) group] can also fulfill the requirement of non-commutativity. This leads to a question of whether an SL(2, \mathbb{C}) gauge field can result in more fruitful topological phase transition phenomena and how such a gauge field can be constructed in experiments. However, for the existing scheme, the spin-flipped hopping terms for different spins are usually not independent, namely they are generated by the same light fields/elements²⁷⁻³³, hence lacking flexibility. This poses challenges in realizing the SL(2, \mathbb{C}) gauge field, which requires a flexible tailoring to achieve independent spin-flipped hopping for different spins. Nevertheless, recent advance in constructing non-Abelian lattice models in photonic synthetic frequency dimensions³³, shows great potential in tackling such a task and exploring the underlying physics of an SL(2, \mathbb{C}) gauge field.

Here, we generalize the SU(2) non-Abelian gauge field (linear superposition of Pauli matrices with real coefficients) to an $SL(2, \mathbb{C})$ one featuring non-Hermitian matrix-form components (complex coefficients), which can be realized by introducing imbalanced spin-flipped

¹State Key Laboratory of Photonics and Communications, School of Physics and Astronomy, Shanghai Jiao Tong University, Shanghai, China. ²Shanghai Research Center for Quantum Sciences, Shanghai, China. ³Collaborative Innovation Center of Light Manipulation and Applications, Shandong Normal University, Jinan, China. —e-mail: yuanlugi@situ.edu.cn

hoppings to the Hamiltonian model in synthetic frequency dimension $^{34-38}$. Such kind of gauge field results in various kinds of transitions of Dirac semimetals 39 , including semimetal-insulator transition, different Dirac-type semimetal transition, annihilation and generation of Dirac points. Furthermore, the imbalanced spin-flipped hopping leads to the intrinsic competition between two hopping mechanisms that results in the transition of the orientation of the edge state projection on the pseudospins, changing from nearly constant to a sinusoidal variation during this process. Moreover, we find that the nontrivial \mathbb{Z}_2 topological phase can be protected by a more generalized symmetry under the SL(2, \mathbb{C}) gauge field. Our work offers the first experimentally feasible proposal to study the underlying physics of SL(2, \mathbb{C}) gauge fields, which enriches the context of topological physics.

Results

Model

We consider the model composed of a one-dimensional ring resonator array including resonant site rings (green) and off-resonant link rings (yellow) in Fig. 1a. Each site ring supports resonant modes at frequencies $\omega_m = \omega_0 + m\Omega$, where ω_0 is the reference frequency and Ω is the frequency spacing. A pair of two coupled site rings (labeled by A and B) can form a photonic molecule 40,41, where each resonant mode at ω_m hybridizes into symmetric and antisymmetric supermodes at $\omega_{m,\pm} = \omega_m \pm \gamma$. Here, γ is the coupling strength between the two rings. Electro-optic modulators (EOMs) are placed in ring A (or B) in the *n*-th photonic molecule at modulation form $J^{A/B}(t) = \pm 2\kappa_{1,n} \cos(\Omega - t)$ $2\gamma t + 2\kappa_{2,n} \cos \Omega t \pm 2\kappa_{3,n} \cos(\Omega + 2\gamma)t$ where $\kappa_{1,n}$, $\kappa_{2,n}$, and $\kappa_{3,n}$ are spatially-dependent modulation strengths. The dynamical modulation on the light field by the EOMs produces sidebands from the original frequency, determined by the modulation frequencies of the modulation signal $f^{A/B}(t)$, and hence connects different frequency modes in the same photonic molecules with frequency spacing $\Omega - 2\gamma$, Ω , and Ω + 2 γ , respectively (details are provided in the Supplemental Note 1).

We assume the spatial spacing between nearby photonic molecules as d, where off-resonant link rings are added to induce spatial coupling $g^{42,43}$. Note that we introduce a small vertical shift on the center of link rings with respect to the center of site rings (see Fig. 1a), and therefore the light propagating from left to right accumulates a

different phase from that of light propagating from right to left (see Supplemental Note 1). The additional propagation phases are expressed by $\alpha_{m,\pm} \propto \phi_m \pm \varphi$ for symmetric and antisymmetric supermodes, with the effective $+(-)\alpha_{m,\pm}$ for the connection from left (right) to right (left) photonic molecules with a multiple of $2\pi^{44}$. Here, $(\phi_m \pm \varphi) \propto (\omega_m \pm \gamma)$ originates from the propagation phase accumulation for all supermodes, where we choose ϕ_m to be multiples of 2π and hence $\alpha \equiv \alpha_{m,+} = \pm \varphi$ for each pair of supermodes.

By further assuming all coupling strengths are relatively small and applying the rotating wave approximation, we obtain the Hamiltonian of the lattice (see Fig. 1b) with $n \, (m)$ being the space (frequency) index in the synthetic space (detailed deviation of the Hamiltonian is provided in Supplemental Note 1):

$$H = \sum_{n,m} \left(c_{m+1,n,+}^{\dagger} c_{m+1,n,-}^{\dagger} \right) \begin{pmatrix} \kappa_{2,n} & \kappa_{3,n} \\ \kappa_{1,n} & \kappa_{2,n} \end{pmatrix} \begin{pmatrix} c_{m,n,+} \\ c_{m,n,-} \end{pmatrix} + g \left(c_{m,n+1,+}^{\dagger} c_{m,n+1,-}^{\dagger} \right) \begin{pmatrix} e^{i\varphi} & 0 \\ 0 & e^{-i\varphi} \end{pmatrix} \begin{pmatrix} c_{m,n,+} \\ c_{m,n,-} \end{pmatrix} + H.c.,$$
(1)

where $c_{m,n,\pm}^{\dagger}$ ($c_{m,n,\pm}$) is the creation (annihilation) operator of the symmetric or antisymmetric supermode at $\omega_{m,\pm}$ for the n-th photonic molecule. Each pair of the symmetric and antisymmetric supermodes can be treated as a pair of pseudospins. The Hamiltonian can be rewritten by

$$H \equiv H_0 + H_1, \tag{2}$$

$$\begin{split} H_{0} &= \sum_{n,m} \left(c_{m+1,n,+}^{\dagger} - c_{m+1,n,-}^{\dagger} \right) (\cos n\theta \sigma_{0} + i \sin n\theta \sigma_{2}) \begin{pmatrix} c_{m,n,+} \\ c_{m,n,-} \end{pmatrix} \\ &+ \left(c_{m,n+1,+}^{\dagger} - c_{m,n+1,-}^{\dagger} \right) (\cos \varphi \sigma_{0} + i \sin \varphi \sigma_{3}) \begin{pmatrix} c_{m,n,+} \\ c_{m,n,-} \end{pmatrix} + H.c., \end{split}$$

$$H_1 = \left(c_{m+1,n,+}^{\dagger} \quad c_{m+1,n,-}^{\dagger} \right) a \sin n\theta \sigma_1 \left(c_{m,n,+} \atop c_{m,n,-} \right) + H.c., \tag{4}$$

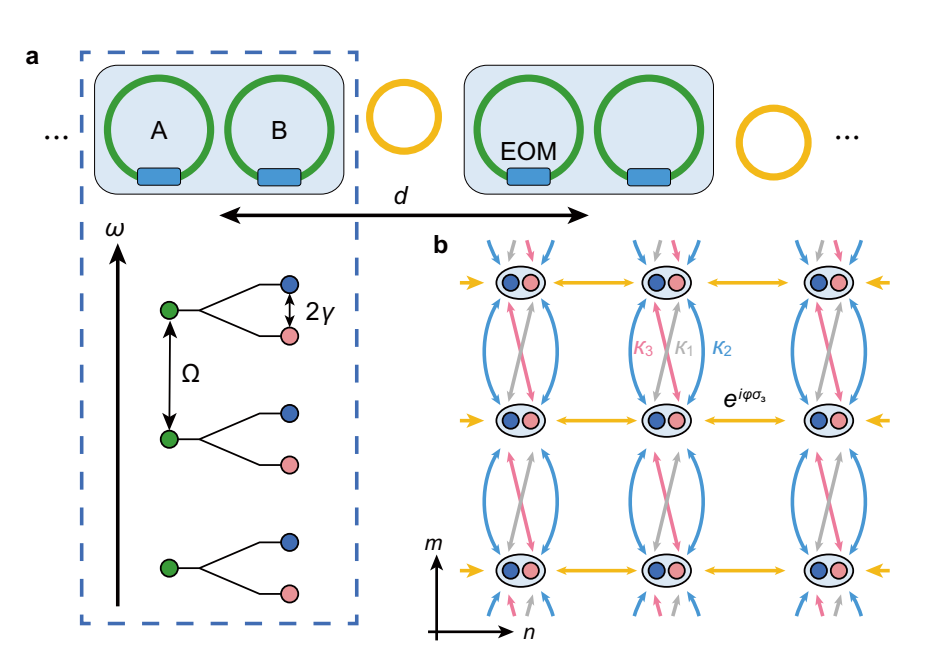


Fig. 1 | The proposed scheme for constructing a two-dimensional non-Abelian lattice gauge field by a photonic molecule array. a Schematic view of the system composed of coupled ring resonators being dynamically modulated by EOMs. The

hybridization of the modes in two individual rings causes a frequency splitting regarding to the original resonant frequency ω_m . **b** Such a system can be mapped to a lattice supporting the two-dimensional Hamiltonian.

where σ_0 , σ_1 , σ_2 , and σ_3 are Pauli matrices, $\kappa_{1,n} \equiv (a-1)\sin n\theta$, $\kappa_{2,n} \equiv \cos n\theta$, $\kappa_{3,n} \equiv (a+1)\sin n\theta$, and g=1 (i.e., the Hamiltonian is dimensionless and all coupling strengths can be scaled versus g, and $a \in R$, $\theta \in [0, 2\pi]$). Importantly, the parameter a represents the imbalance between the pseudospin-dependent spin-flipped hopping term, namely, $|\kappa_{1,n}| - |\kappa_{3,n}| = 2a\sin n\theta$ (for $0 \le a \le 1$), which modifies the hopping along the frequency dimension from an SU(2) type of matrix to an SL(2, $\mathbb C$) one, and correspondingly marks the appearance of an SL(2, $\mathbb C$) gauge potential. The corresponding non-Abelian gauge field is written by

$$\mathbf{A} \equiv \begin{cases} (A_{f,\uparrow}, A_{x}) = (\eta(\theta)\sigma_{2} - ia\eta(\theta)\sigma_{1}, \varphi\sigma_{3}) \\ (A_{f,\downarrow}, A_{x}) = (\eta(\theta)\sigma_{2} + ia\eta(\theta)\sigma_{1}, \varphi\sigma_{3}) \end{cases},$$
 (5)

where $A_{\mathbf{f},\uparrow}$ $(A_{\mathbf{f},\downarrow})$ is the gauge field component along the positive (negative) direction along the frequency axis, $\eta(\theta) = \frac{1}{2\sqrt{a^2-1}}\log\frac{\cos n\theta+\beta}{\cos n\theta-\beta}$, and $\beta = \sqrt{(a^2-1)\sin^2 n\theta}$. One can see the component $A_{\mathbf{f},\uparrow}$ $(A_{\mathbf{f},\downarrow})$ gives the hopping that mixes the pseudospins along frequency dimension, while the component $A_{\mathbf{x}}$ provides an opposite hopping phase $\pm \varphi$ along spatial dimension. In particular, \mathbf{A} does not belong to an SU(2) gauge potential when $a \neq 0$ due to the appearance of the non-Hermitian matrix $-ia\eta(\theta)\sigma_1$ in $A_{\mathbf{f},\uparrow}$ $(A_{\mathbf{f},\downarrow})$, instead, it refers to an SL(2, \mathbb{C}) gauge potential, which is a complex generalization of the SU(2) one (see Supplemental Note 2). Note that the asymmetric gauge field

component $A_{f,\uparrow}$ ($A_{f,\downarrow}$) preserves the Hermiticity of the Hamiltonian.

Annihilation of Dirac points and rotation of pseudospin

We investigate how the bandstructure changes when $a \neq 0$, for the Hamiltonian under the non-Abelian magnetic flux $(\theta, \varphi) = (2\pi/3, \pi/2)$ (so the lattice has the period of $2\pi/\theta = 3$ along the spatial axis). In Fig. 2a, b, we show the band structures of H with a = 0 and a = 1 (see "Methods" for the Bloch Hamiltonian in the reciprocal space), where $k_{\rm f}(k_{\rm x})$ is the quasi-momentum reciprocal to the frequency (space) axis and ε is the quasienergy. The six bands are separated, labeled from 1–6,

which reflects the non-Abelian nature of the gauge field (see Supplemental Note 3). When a = 0, there are four band-crossing points between band 4 and band 5 in Fig. 2a, which refer to type-I Dirac points³⁹. However, when a = 1, there is only a trivial gap between band 4 and band 5 in Fig. 2b, indicating a semimetal-insulator transition. Different Dirac-type semimetal transition and topological-normal insulator transition can also be presented if one chooses different flux (θ, ω) (see Supplemental Note 4).

Properties of edge states with a spatial open boundary condition for N=31 sites are investigated. We define a quantity $\Lambda=|v_{n_b}|^2/\sum_n|v_n|^2$ to characterize the localization amplitude of an eigenstate v on the edge, where $n_b=1$ or 31 labels one edge. Furthermore, we define the edge-state pseudospin projection (ESPP) as $\langle \sigma_i \rangle = \left\langle v_{n_b} |\sigma_i| v_{n_b} \right\rangle$, which partially reflects the changes in the spin-orbit coupling of the Hamiltonian H

When a = 0, the Dirac points in Fig. 2a are located at $k_f \Omega = 0.8\pi$ and 1.2π . There are four bands that support large localization Λ for a range of $k_{\rm f}$, indicating the corresponding edge localization (see Fig. 2d), where two of them (labeled in blue and red) are merged into the upper bulk bands for k_f out of two Dirac points and the other two (labeled in green and yellow) belong to edge states. Two dips in the curves of Λ appear in the vicinity of the Dirac points as bulk bands close into the degeneracy at the Dirac points, so edge modes do not hold the localization feature at the two dips (see Supplemental Note 5). The distribution of the pseudospin for the upper blue band and lower green band is given in Fig. 2e, f, respectively. The upper red band (bottom yellow band) has the opposite distribution of the ESPP $\langle \sigma_i \rangle$ over the entire $k_{\rm f}$ as the one for the upper blue band (bottom green band). The ESPP $\langle \sigma_i \rangle$ for these two bands is nearly a constant with respect to $k_{\rm f}$, so the ESPP is pinned at the y-axis in the Bloch sphere with $k_{\rm f}$ varying, except for a sudden jump to the z-axis when $k_f\Omega = 0$ and π due to the vanishing of the spin-orbit coupling term $\sigma_2 k_{\rm f}$ (see Supplemental Note 6). As a increases, the Dirac points move closer to each other, then merge at about a = 0.55, and finally vanish due to their opposite Berry curvature (see Supplemental Note 7), resulting in gap opening. as illustrated in Fig. 2c. The additional spin-flipped hopping (i.e., the

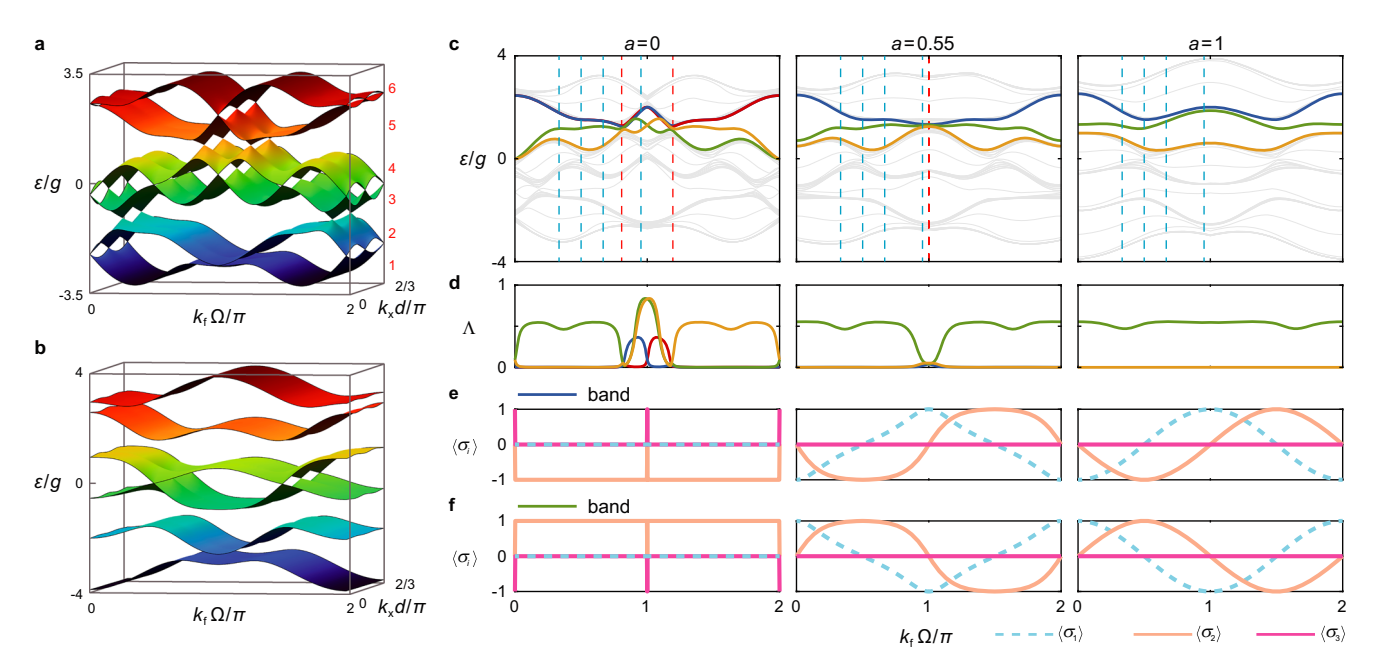


Fig. 2 | The annihilation of the Dirac points with the changes of the localization features at the edge and the variation of ESPP. Bandstrucutre of the model H in Eq. (2) by varying a from (a) a=0 to (b) a=1. Red numbers in a denote the band labels. c Projected bandstructure with different strengths of the spin-flipped hopping a. Red dashed lines denote the position of the Dirac points, which correspond

to $k_i\Omega$ = 0.8 π , 1.2 π and $k_i\Omega$ = π , respectively. Blue dashed lines denote the corresponding momenta in Fig. 3. **d** The quantity Λ for the localization of the edge states. The colors of the lines are in accordance with the colored bands in (**c**). **e**, **f** ESPP $\langle \sigma_i \rangle$ of the blue band and green band in (**c**), respectively.

term with $a \neq 0$) also causes the hybridization between green and vellow bands and the hybridization between blue and red bands (see Supplemental Note 6), where the former hybridization results in the monomorphic edge band and the latter one pushes one of the resulting band into the upper bulk (so the red band is not shown for $a \neq 0$). One can see, at a = 0.55 (Fig. 2c), the Dirac points get close to each other near $k_f \Omega = \pi$, and Λ of the edge state is nearly 0 in the vicinity of $k_f\Omega = \pi$. When $a \neq 0$ and such hybridization occurs, the ESPP $\langle \sigma_i \rangle$ at the vicinity of $k_f \Omega = 0$ and π is modified, and so the ESPP is rotated in the xy-plane of the Bloch sphere with a non-constant velocity by varying $k_{\rm f}$. As a further increase to 1, which marks the largest imbalance between the spin-flipped hopping terms $\kappa_{1,n} = 0$, and $\kappa_{3,n} = 2 \sin n\theta$ the Dirac points merge and the gap opens with an edge state showing the localization feature throughout the entire $k_{\rm f}$. Moreover, the ESPP $\langle \sigma_i \rangle$ of the two bands becomes a sinusoidal form in Fig. 2d-f, corresponding to a rotation of the ESPP with a constant velocity. We find a similar change of the ESPP under different choices of (θ, φ) when a varies from 0 to 1 (see Supplemental Note 8).

The additional spin-flipped hopping term with $a \neq 0$ hybridizes the bands and consequently modifies the pseudospin of the eigenstates regardless of the non-Abelian flux (i.e., the values of θ and φ). To further investigate such a pseudospin rotation phenomenon, we perform the numerical simulation of the evolution with a being adiabatically decreased from 1 to 0 in Fig. 3, with the choice of N = 19 (details of the simulation is given in Supplemental Note 9).

We choose four different states on the green bands with $k_f\Omega = \pi/3$, $\pi/2$, $2\pi/3$, and $20\pi/21$, tuned from a = 1 to a = 0 with the bandstructures given in Fig. 2c. When $0 \le t \le 50g^{-1}$, we keep a = 1 to excite the desired eigenstate. After $t = 50g^{-1}$, a is linearly changed from 1 to 0. One can find that even though the four states start with different pseudospins, they all converge to the one with $\sigma_2 = 1$ at $t = 200g^{-1}$ (see Fig. 3a-d), which indicates how the additional spin-flipped hopping term gradually rotates the pseudospin of the eigenstate. We also show the evolution of the spatial intensity of all frequency modes on each spatial site in Fig. 3e-h. Despite the rotations in pseudospin, the spatial intensities are almost unchanged and localized at the edge in Fig. 3e-g. However, for the case of $k_f\Omega = 20\pi/21$ in Fig. 3h, the state exhibits a transition starting with an edge state, then to a bulk state, and finally becoming an edge state located at the other side. Such different dynamics occur due to the fact of different occupation of choices of $k_{\rm f}\Omega = \pi/3$, $\pi/2$, $2\pi/3$ and the choice of $k_{\rm f}\Omega = 20\pi/21$ appearing on different sides of the Dirac point at $k_f\Omega = 0.8\pi$ while one tunes a from 1 to 0 (see Fig. 2c). Therefore, when $k_{\rm f}$ crosses the Dirac point in Fig. 2c, the edge state crosses through the bulk towards the other edge adiabatically. Note that if the evolution time is too short, the adiabatic approximation cannot be maintained, resulting in the inefficient transition to the target eigenstates (see Supplemental Note 9).

Phase transition in the (a, b) plane

One sees that there are two kinds of spin-flipped hopping terms $i \sin n\theta \sigma_2$, and $a \sin n\theta \sigma_1$ in H, while we only tune the lateral one in the above cases. The independent coupling strengths $\kappa_{1,n}$ and $\kappa_{3,n}$ allow us to make the other one also tunable by manipulating $\kappa_{1,n} \equiv (a-b) \sin n\theta$, $\kappa_{3,n} \equiv (a+b) \sin n\theta$ where b is a real number, and hence the Hamiltonian H is extended to a more general one H' with a modified $\mathrm{SL}(2,\mathbb{C})$ gauge field \mathbf{A}' (see Supplemental Note 2).

Different Dirac point transitions between the fourth band and fifth band through changing both parameters a and b are illustrated by the phase diagram in Fig. 4. One see that there are always four type-I Dirac points between the fourth and fifth band under an SU(2) gauge field (line a = 0). While for the SL(2, $\mathbb C$) gauge field [the (a,b) plane], various transitions between six different phases are involved, which indicates the intriguing opportunities in topological physics with SL(2, $\mathbb C$) gauge field.

As an example, we show the phase transition from type-I to type-II Dirac points with a = b fixed, where only the spin-flipped hopping $(\kappa_{3,n})$ between $c_{m,n,-}$ and $c_{m+1,n,+}$ is allowed, while the other one between $c_{m,n,+}$ and $c_{m+1,n,-}$ is prohibited ($\kappa_{1,n} = 0$). For a = 0, the model degrades to the Abelian gauge-field case without the spin-flipped hopping terms, and two degenerated edge states with opposite ESPP $\sigma_3 = \pm 1$ link the Dirac points (see Fig. 5a). As a slightly increases to 0.1, the corresponding gauge field becomes non-Abelian, and the degeneracy of the two bands is lifted. In contrast to the cases we study in Fig. 2, the ESPP of the bands changes abruptly to a sinusoidal form, as shown in Fig. 5c, d. If a further increase to 0.5, one can find that both the position and the tilt of Dirac cones are changed, which gives the type-II Dirac points (see Fig. 5a and Supplemental Note 10 for the bandstructures). The ESPP for a = b = 0.5remains the same as the ones for a = b = 0.1, which implies the sinusoidal varying ESPPs are the result of the balance between the two kinds of hopping mechanisms associated with a and b in the spin-flipped hopping terms (see "Methods"). To get a better insight, we consider the reciprocal space. The term $a\sin n\theta\sigma_1\propto\cos k_{\rm f}$ (or the other term $ib \sin n\theta \sigma_2 \propto \sin k_f$) with corresponding eigenvectors same as σ_1 (or σ_2), so the effect of the spin-flipped hopping becomes strongest at $k_f\Omega = 0$, π (or $k_f\Omega = 0.5\pi$, 1.5π) and vanishes at $k_f\Omega = 0.5\pi$, 1.5π (or $k_{\rm f}\Omega = 0$, π). As a consequence of the competition between these two

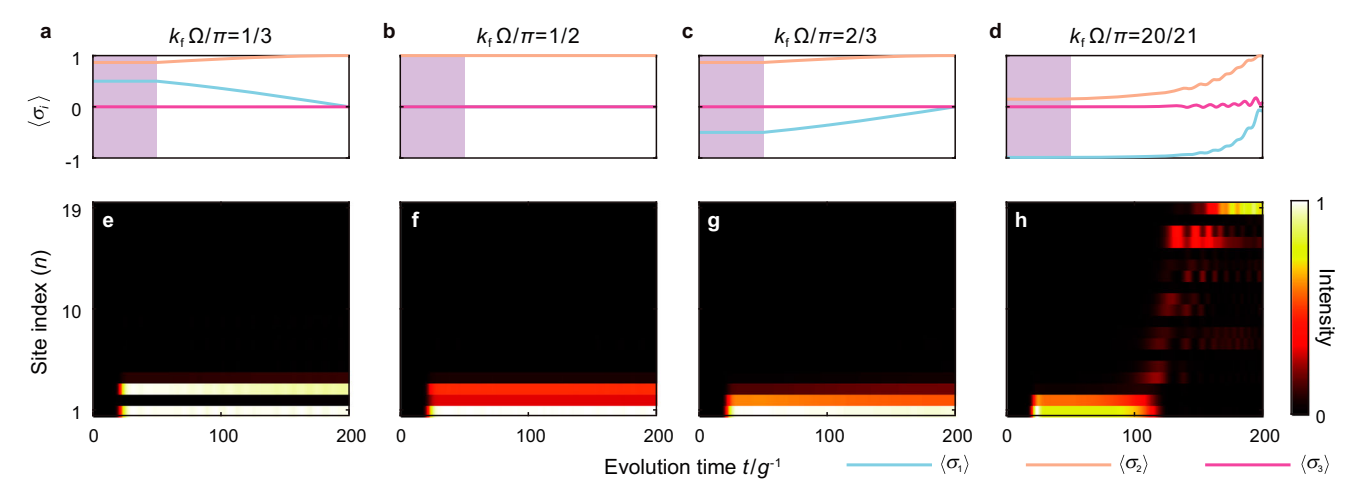


Fig. 3 | **Adiabatic evolution of ESPP and the intensity distribution for different states. a–d** Temporal evolutions with a tuned from 1 to 0 adiabatically of the pseudospin $\langle \sigma_i \rangle$ of the states with different $k_{\rm f}$. Violet regions show the time interval

with a being kept as 1 to excite the desired eigenstate. **e**-**h** Temporal evolution of the total intensity over all frequency modes versus each spatial site n with different choices of $k_{\rm f}$.

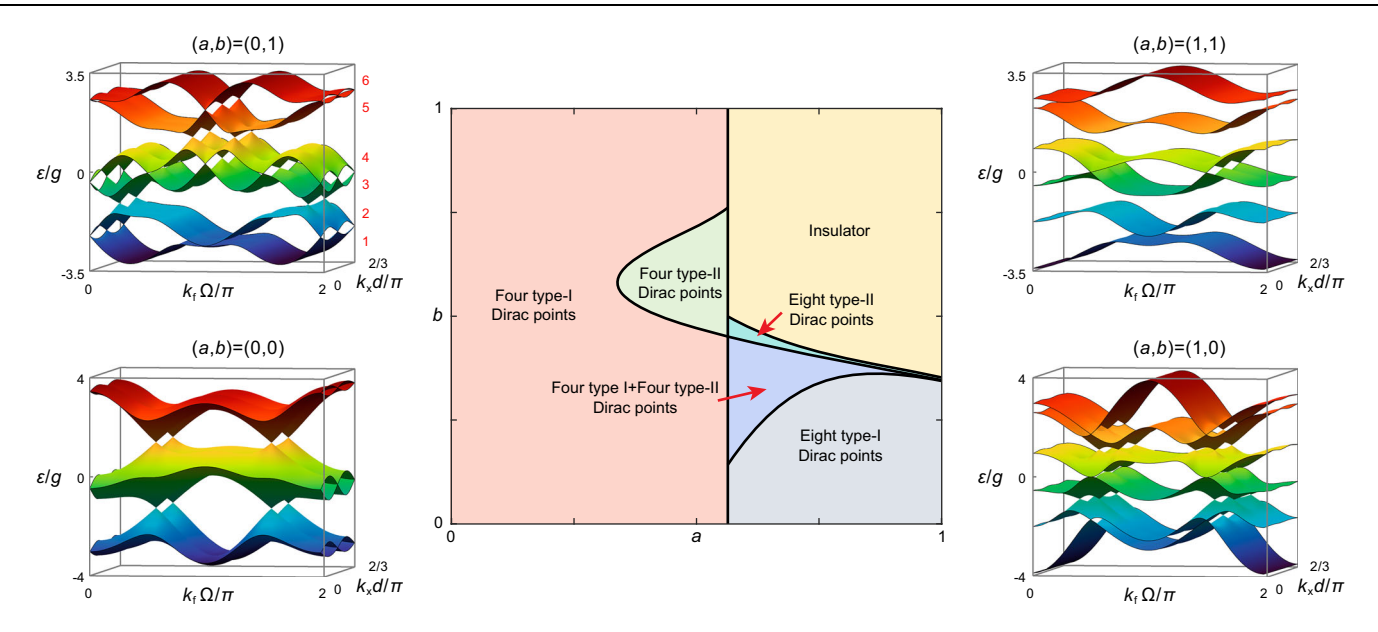


Fig. 4 | **Various phase transitions in the** (a, b) **plane.** Phase diagram under different choices of the parameters a and b. Bandstructures of the model H' for different (a, b) in spin-flipped hopping terms with (θ , φ) = ($2\pi/3$, $\pi/2$).

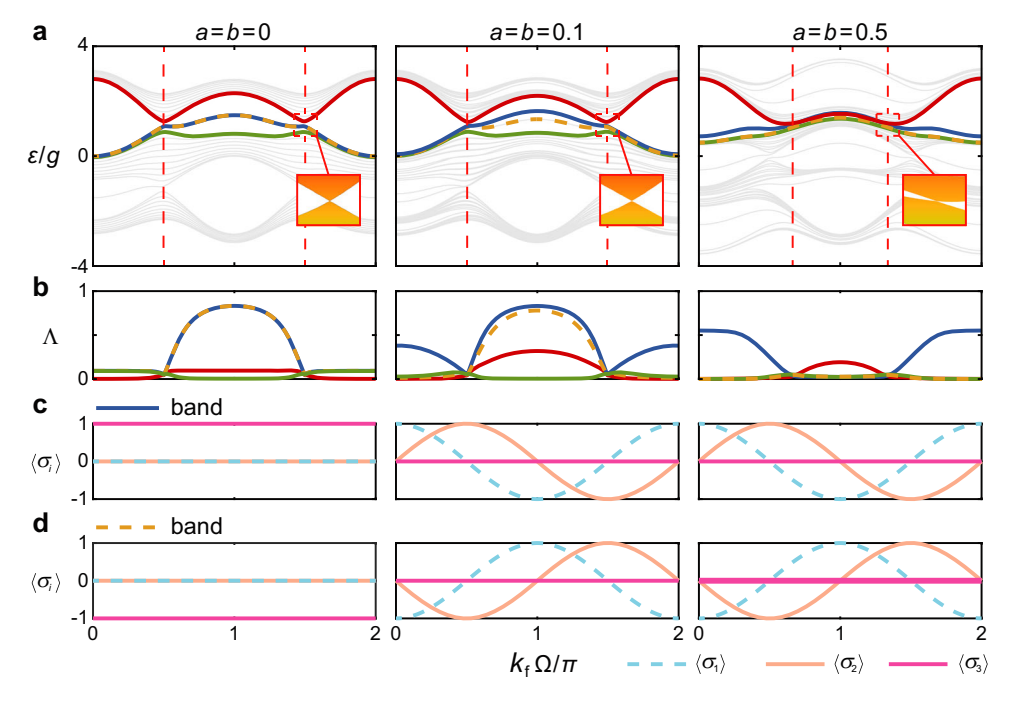


Fig. 5 | Transition from type-I Dirac points to type-II Dirac points with the changes with the localization features at the edge and the variation of ESPP. a Projected bandstructure with different strengths of the spin-flipped hopping a and b. Red dashed lines denote the position of the Dirac points. Inserted figures show the

bandstructure at the vicinity of the Dirac points with the periodic boundary condition taken in both space and frequency dimensions. **b** The quantity \varLambda for the localization of the edge states. The colors of lines are in accordance with the colored bands in (**a**), **c**, **d** ESPP $\langle \sigma_i \rangle$ of the blue band and green band in (**a**), respectively.

mechanisms from spin-flipped hopping terms, the orientation of the ESPP rotates in the xy-plane as k_f varies, which implies one can possibly have a k_f -dependent pseudospin beyond sinusoidal variation by a delicate design of the spin-flipped hopping terms.

Difference between SL(2, C) and SU(2) gauge fields

To further illustrate the difference between the SL(2, \mathbb{C}) gauge field and the SU(2) gauge field, we consider an Abelian example with $(\theta, \varphi) = (2\pi/3, \pi)$, where the effect of the non-Abelian gauge field is excluded, and the phase transition process is fully attributed to an SL(2, \mathbb{C}) gauge field. The energy spectrum of the Hamiltonian H is

plotted in Fig. 6a with a varying from 0 to 1. One sees that there is no gap closing during this process, which usually denotes the absence of a topological phase transition. However, the \mathbb{Z}_2 topological invariant ν is changed from 1 to 0 (see Supplemental Note 8).

Typical bandstructures are given in Fig. 6a, b with (a, b) = (0, 1) (topological nontrivial) and (a, b) = (1, 1) (topological trivial). Moreover, we find that such a phase transition occurs immediately once $a \neq 0$, indicating that the symmetry which protects the nontrivial topological phase is broken by the introduction of the SL(2, \mathbb{C}) gauge field. Note that for an SU(2) gauge field, the hopping term U is an SU(2) matrix, and the spin-flipped hopping terms satisfy an anti-conjugate

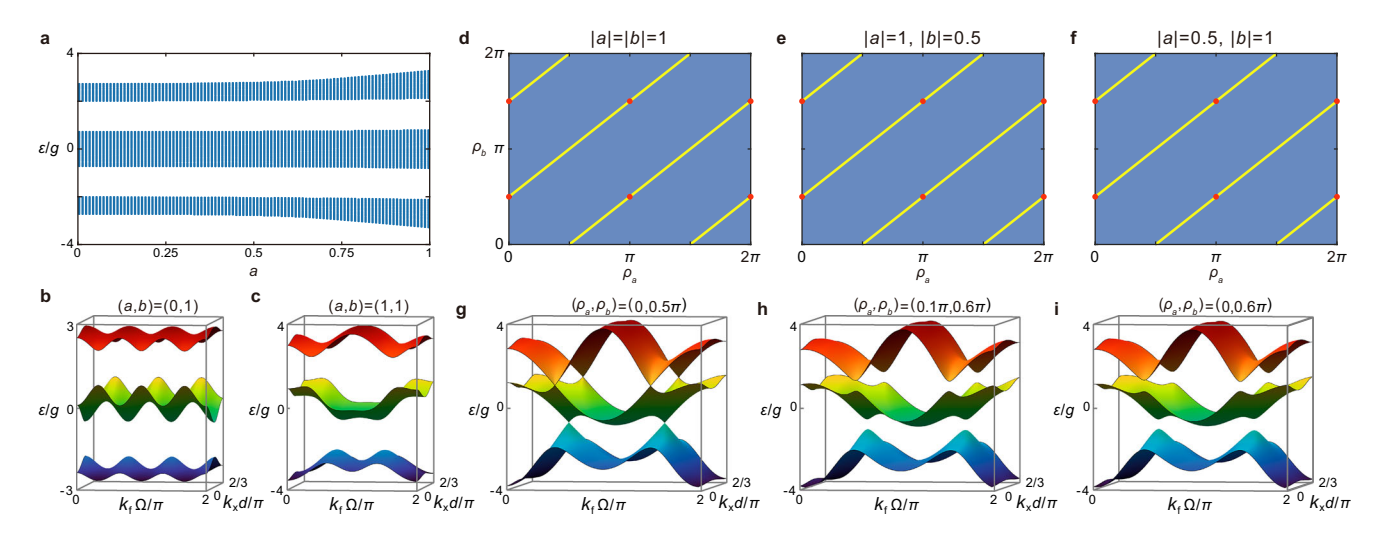


Fig. 6 | **Topological phase transition under SL(2,** \mathbb{C}) **gauge fields. a** Energy spectrum of the Hamiltonian $H_{\mathbf{k}}$, **b**, **c** Bandstructures of the Hamiltonian $H_{\mathbf{k}}$ with (a,b)=(0,1) and (a,b)=(1,1). **d-f** Phase diagrams in the (ρ_a,ρ_b) plane for the model with different choices of |a| and |b|, where the yellow lines denote the non-trivial

phase with a \mathbb{Z}_2 topological invariant $\nu=1$, while the blue regions correspond to a topological trivial phase with $\nu=0$. Red dots denote the values of ρ_a and ρ_b when four-fold band-crossing points appear. **g**-**i** The corresponding band structures with |a|=|b|=1 and a different choice of ρ_a and ρ_b .

relation $U_{12} = -U_{21}^{*45}$, while the variation of the parameter a breaks this condition. To further investigate such a phase transition process, we now define a and b as two complex numbers $a = |a|e^{i\rho_a} b = |b|e^{i\rho_b}$. The phase diagram for |a| = |b| = 1 is plotted in Fig. 6d. The blue region (topological trivial phase with v = 0) covers most of the area in the phase diagram, and the nontrivial phase with v=1 occurs at $\rho_a = \rho_b \pm 0.5\pi$ and $\rho_a = \rho_b \pm 1.5\pi$, denoted by the yellow lines. Similar phase diagrams are also found for $|a| \neq |b|$ as shown in Fig. 6e, f. Moreover, in the (ρ_a, ρ_b) plane, the corresponding bandstructure always shows an insulator phase except for $(\rho_a, \rho_b) = (0, \pm 0.5\pi)$ and $(\rho_a, \rho_b) = (\pi, \pm 0.5\pi)$ denoted by the red dots, where the gaps close and four-fold band-crossing points appear (e.g., Fig. 6g). Typical bandstructures for the topological nontrivial phase and the topological trivial phase are given in Fig. 6h, i with $(\rho_a, \rho_b) = (0.1\pi, 0.6\pi)$ and $(\rho_a, \rho_b) = (0, 0.6\pi)$. One can rewrite the condition for the topological nontrivial phase as $|\kappa_{1,n}| = |\kappa_{3,n}|$ or equivalently $|U_{12}| = |U_{21}|$. In other words, the symmetry that protects the nontrivial topological phase under an SU(2) gauge field is broken by the introduction of an SL(2, \mathbb{C}) gauge field, but it can be retrieved in a more generalized form under an SL(2, ℂ) gauge field.

Discussion

Our proposal can be feasible for experimental demonstrations. The fiber optic system could be a potential candidate as the combination of photonic molecules and synthetic frequency dimension⁴⁶⁻⁴⁸ have already been demonstrated in experiments, which provide the building block of our theoretical proposal. Specifically, for a fiberbased experimental setup with a cavity free spectral range ~10MHz and cavity length ~10m, the required amplitude of the voltage signal sent to the EOMs is ~1V^{46,48}. The quality factor of the cavities ideally desires an order of magnitude ~109 to avoid the over-broadening of bands, which is challenging, but can be potentially doable with the development of state-of-art photonic technologies^{48,49} (see Supplemental Note 11). A precise control on the modulation depth and frequency of the EOMs is required to minimize the distortion of the measured bandstructure (see Supplemental Note 12). The disorder in the coupling between the rings can lead to the inefficient excitation of the edge state in experimental observation (see Supplemental Note 13). On the other hand, in the field of integrated photonics, the photonic molecule 41,50 and synthetic frequency dimension 51-53 have been individually experimentally demonstrated for on-chip ring

resonators. Moreover, a recent experiment⁵⁴ also shows the possibility to introduce synthetic frequency dimension in a one-dimensional ring resonator array. All these state-of-art nanophotonic technologies provide the potential to realize our proposal in the near future.

In summary, we extend SU(2) non-Abelian gauge fields to the $SL(2,\mathbb{C})$ regime, and give a theoretical proposal for simulating topological materials under such a gauge field. The underlying physics is unveiled in two aspects: various Dirac phase transitions beyond the conventional SU(2) gauge field and the transition of the orientation of the ESPP. Moreover, the extension to SL(2, C) gauge field unveils a more generalized symmetry that protects the nontrivial \mathbb{Z}_2 topological phase. We expect the proposed system to be a unique and versatile platform for studying topological physics with non-Abelian gauge fields. Future studies may include the employment of the non-Abelian topological charge^{55,56}, which describes the topology of multiband systems, offering a useful tool to elucidate the nature of the phase transition discussed. The proposed system may also find potential applications on topological insulator lasers in synthetic space-frequency dimensions^{57,58} from pseudospin manipulations via introducing an SL(2, C) gauge field, which provides an extra degree of freedom to modify the spectrotemporal shape of the output pulses.

Methods

Bloch Hamiltonian in the reciprocal space

We assume θ satisfies $\theta = 2\pi/P$, where P is an integer, and therefore, the system can still maintain periodicity in both the spatial and frequency dimensions. For the choice of $\theta = 2\pi/3$, the lattice has a period of $2\pi/\theta = 3$ along the spatial axis, as the hopping along the frequency dimension (associated with θ) depends on the spatial index n. The Bloch Hamiltonian in the reciprocal space is then given by (detailed derivation for other choices of θ is given in the Supplemental Note 1)

$$H_{\mathbf{k}} = \left(c_{\mathbf{k},1,+}^{\dagger} c_{\mathbf{k},1,-}^{\dagger} c_{\mathbf{k},2,+}^{\dagger} c_{\mathbf{k},2,-}^{\dagger} c_{\mathbf{k},3,+}^{\dagger} c_{\mathbf{k},3,-}^{\dagger}\right) \\ \tilde{H}_{\mathbf{k}} \left(c_{\mathbf{k},1,+} c_{\mathbf{k},1,-} c_{\mathbf{k},2,+} c_{\mathbf{k},2,-} c_{\mathbf{k},3,+} c_{\mathbf{k},3,-}\right)^{T},$$
(6)

$$\tilde{H_{\mathbf{k}}} = \begin{pmatrix} B_1(k_{\mathrm{f}},\theta) & C_1(k_{\mathrm{f}},\theta) & e^{i\varphi}e^{-ik_{\mathrm{x}}d} & 0 & e^{-i\varphi}e^{ik_{\mathrm{x}}d} & 0 \\ C_1^*(k_{\mathrm{f}},\theta) & B_1(k_{\mathrm{f}},\theta) & 0 & e^{-i\varphi}e^{-ik_{\mathrm{x}}d} & 0 & e^{i\varphi}e^{ik_{\mathrm{x}}d} \\ e^{-i\varphi}e^{ik_{\mathrm{x}}d} & 0 & B_2(k_{\mathrm{f}},\theta) & C_2(k_{\mathrm{f}},\theta) & e^{i\varphi}e^{-ik_{\mathrm{x}}d} & 0 \\ 0 & e^{i\varphi}e^{ik_{\mathrm{x}}d} & C_2^*(k_{\mathrm{f}},\theta) & B_2(k_{\mathrm{f}},\theta) & 0 & e^{-i\varphi}e^{-ik_{\mathrm{x}}d} \\ e^{i\varphi}e^{-ik_{\mathrm{x}}d} & 0 & e^{-i\varphi}e^{ik_{\mathrm{x}}d} & 0 & B_3(k_{\mathrm{f}},\theta) & C_3(k_{\mathrm{f}},\theta) \\ 0 & e^{-i\varphi}e^{-ik_{\mathrm{x}}d} & 0 & e^{i\varphi}e^{ik_{\mathrm{x}}d} & C_3^*(k_{\mathrm{f}},\theta) & B_3(k_{\mathrm{f}},\theta) \end{pmatrix}$$

where $B_j(k_{\rm f},\theta) = 2\cos j\theta\cos k_{\rm f}\Omega$, $C_j(k_{\rm f},\theta) = 2a\sin j\theta\cos k_{\rm f}\Omega - 2i\sin j\theta\sin k_{\rm f}\Omega$, and j=1,2,3 being the index of the sites in the reciprocal space. By diagonalizing $H_{\bf k}$, one can obtain the bandstructure. One can also rewrite $\tilde{H}_{\bf k}$ in spin-orbit coupling form

$$\tilde{H}_{\mathbf{k}} = \begin{pmatrix} D_1(k_{\mathrm{f}}, \theta) & e^{i\varphi\sigma_3}e^{-ik_{\mathrm{x}}d} & e^{-i\varphi\sigma_3}e^{ik_{\mathrm{x}}d} \\ e^{-i\varphi\sigma_3}e^{ik_{\mathrm{x}}d} & D_2(k_{\mathrm{f}}, \theta) & e^{i\varphi\sigma_3}e^{-ik_{\mathrm{x}}d} \\ e^{i\varphi\sigma_3}e^{-ik_{\mathrm{x}}d} & e^{-i\varphi\sigma_3}e^{ik_{\mathrm{x}}d} & D_3(k_{\mathrm{f}}, \theta) \end{pmatrix}, \tag{8}$$

where $D_j(k_f,\theta) = 2\cos j\theta \cos k_f\Omega\sigma_0 + 2a\sin j\theta \cos k_f\Omega\sigma_1 + 2\sin j\theta \sin k_f\Omega\sigma_2$ following the form of typical spin-orbit terms ⁵⁹. The last two terms in $D_j(k_f,\theta)$ correspond to the two different spin-flipped hopping mechanisms.

Quantitative analysis on the ESPP

To quantitatively analyze the change of pseudospin behaviors originating from the competition between the two spin-flipped hopping mechanisms. We consider a simplified model, which also exhibits the same pseudospin behaviors as *H*. The Hamiltonian is read as

$$H_{s} = \sum_{m} \left(c_{m+1,+}^{\dagger} c_{m+1,-}^{\dagger} \right) \begin{pmatrix} \cos \theta & 0 \\ 0 & \cos \theta \end{pmatrix} \begin{pmatrix} c_{m,+} \\ c_{m,-} \end{pmatrix}$$

$$+ \left(c_{m+1,+}^{\dagger} c_{m+1,-}^{\dagger} \right) \begin{pmatrix} 0 & a \sin \theta \\ a \sin \theta & 0 \end{pmatrix} \begin{pmatrix} c_{m,+} \\ c_{m,-} \end{pmatrix}$$

$$+ \left(c_{m+1,+}^{\dagger} c_{m+1,-}^{\dagger} \right) \begin{pmatrix} 0 & b \sin \theta \\ b \sin \theta & 0 \end{pmatrix} \begin{pmatrix} c_{m,+} \\ c_{m,-} \end{pmatrix} + H.c.,$$

$$(9)$$

where the second and third terms correspond to the two hopping mechanisms, respectively. One can obtain the eigenstate of the Hamiltonian by diagonalizing $H_{\rm S}$

$$|\psi\rangle = \frac{1}{|\psi|} \left(\pm \sqrt{\frac{a\cos k - ib\sin k}{a\cos k + ib\sin k}}, 1 \right)^{T}, \tag{10}$$

where $|\psi|$ is the normalization factor. One can further obtain the pseudospin projection $\langle \sigma_i \rangle$. We take $\langle \sigma_1 \rangle$ as an example

$$\left\langle \sigma_{1}\right\rangle =\left\langle \psi_{+}\left|\sigma_{1}\right|\psi_{+}\right\rangle =\frac{1}{\left|\psi\right|^{2}}\left(\sqrt{\frac{a\cos k-ib\sin k}{a\cos k+ib\sin k}}+\sqrt{\frac{a\cos k+ib\sin k}{a\cos k-ib\sin k}}\right).\tag{11}$$

We first consider the two special cases. For a=0 and b=1, $\langle \sigma_1 \rangle = 0$; for a=1 and b=1, $\langle \sigma_1 \rangle = \cos k$, which are in accordance with our model. To further illustrate the competition between the two hopping mechanisms, we consider a perturbative case, where b=1 and $a \ll 1$. In this case

$$\langle \sigma_1 \rangle = \frac{1}{|\psi|^2} \left(\sqrt{1 + \frac{-2ib\sin k}{a\cos k + ib\sin k}} + \sqrt{1 + \frac{2ib\sin k}{a\cos k - ib\sin k}} \right), \quad (12)$$

One sees that $\langle \sigma_1 \rangle$ depends on the values of $a \cos k$ and $b \sin k$. For k=0 and $k=\pi$, the nominator parts are vanished as $b \sin k=0$, so $\langle \sigma_1 \rangle = 1$, while for $k \gg 0$, $\langle \sigma_1 \rangle \to 0$ as $a \cos k \to 0$. Therefore, there are two peaks located at k=0 and $k=\pi for \langle \sigma_1 \rangle$, which can also be found in the Supplemental Note 6.

Data availability

The data generated in this study have been deposited in the Figshare database under accession code [https://doi.org/10.6084/m9.figshare. 29714342].

Code availability

The codes used to process the data generated in this study are available in Figshare under accession code [https://doi.org/10.6084/m9.figshare.29714342].

References

- Dalibard, J., Gerbier, F., Juzeliūnas, G. & Öhberg, P. Colloquium: artificial gauge potentials for neutral atoms. Rev. Mod. Phys. 83, 1523 (2011).
- Goldman, N., Juzeliūnas, G., Öhberg, P. & Spielman, I. B. Lightinduced gauge fields for ultracold atoms. Rep. Prog. Phys. 77, 126401 (2014).
- Aidelsburger, M., Nascimbene, S. & Goldman, N. Artificial gauge fields in materials and engineered systems. *Comptes Rendus Phys.* 19, 394 (2018).
- 4. Wu, T. T. & Yang, C. N. Concept of nonintegrable phase factors and global formulation of gauge fields. *Phys. Rev. D.* **12**, 3845 (1975).
- Wilczek, F. & Zee, A. Appearance of gauge structure in simple dynamical systems. *Phys. Rev. Lett.* 52, 2111 (1984).
- Horváthy, P. Non-abelian Aharonov-Bohm effect. Phys. Rev. D. 33, 407 (1986).
- 7. Yan, Q. et al. Non-abelian gauge field in optics. *Adv. Opt. Photonics* **15**, 907 (2023).
- 8. Yang, Y. et al. Non-abelian physics in light and sound. Science **383**, eadf9621 (2024).
- Zhang, P.-M. & Horvathy, P. Isospin precession in non-abelian Aharonov-Bohm scattering. Preprint at arXiv https://doi.org/10. 48550/arXiv.2402.13883 (2024).
- Osterloh, K., Baig, M., Santos, L., Zoller, P. & Lewenstein, M. Cold atoms in non-abelian gauge potentials: From the Hofstadter "moth" to lattice gauge theory. *Phys. Rev. Lett.* 95, 010403 (2005).
- Satija, I. I., Dakin, D. C. & Clark, C. W. Metal-insulator transition revisited for cold atoms in non-abelian gauge potentials. *Phys. Rev. Lett.* 97, 216401 (2006).
- Goldman, N., Kubasiak, A., Gaspard, P. & Lewenstein, M. Ultracold atomic gases in non-abelian gauge potentials: the case of constant Wilson loop. *Phys. Rev. A* 79, 023624 (2009).
- Goldman, N. et al. Non-abelian optical lattices: anomalous quantum hall effect and dirac fermions. Phys. Rev. Lett. 103, 035301 (2009).
- Goldman, N. et al. Realistic time-reversal invariant topological insulators with neutral atoms. Phys. Rev. Lett. 105, 255302 (2010).
- Hauke, P. et al. Non-abelian gauge fields and topological insulators in shaken optical lattices. Phys. Rev. Lett. 109, 145301 (2012).
- Burrello, M., Fulga, I., Alba, E., Lepori, L. & Trombettoni, A. Topological phase transitions driven by non-abelian gauge potentials in optical square lattices. *Phys. Rev. A* 88, 053619 (2013).
- Kosior, A. & Sacha, K. Simulation of non-abelian lattice gauge fields with a single-component gas. Europhys. Lett. 107, 26006 (2014).
- Lepori, L., Fulga, I. C., Trombettoni, A. & Burrello, M. Double Weyl points and fermi arcs of topological semimetals in non-abelian gauge potentials. *Phys. Rev. A* 94, 053633 (2016).
- 19. Yang, Y., Zhen, B., Joannopoulos, J. D. & Soljačić, M. Non-abelian generalizations of the Hofstadter model: spin-orbit-coupled butterfly pairs. *Light.: Sci. Appl.* **9**, 177 (2020).
- Di Liberto, M., Goldman, N. & Palumbo, G. Non-abelian Bloch oscillations in higher-order topological insulators. *Nat. Commun.* 11, 5942 (2020).
- Wunderlich, J., Kaestner, B., Sinova, J. & Jungwirth, T. Experimental observation of the spin-Hall effect in a two-dimensional spin-orbit

- coupled semiconductor system. *Phys. Rev. Lett.* **94**, 047204 (2005).
- 22. Ruseckas, J., Juzeliūnas, G., Öhberg, P. & Fleischhauer, M. Nonabelian gauge potentials for ultracold atoms with degenerate dark states. *Phys. Rev. Lett.* **95**, 010404 (2005).
- 23. Abdumalikov Jr, A. A. et al. Experimental realization of non-abelian non-adiabatic geometric gates. *Nature* **496**, 482 (2013).
- 24. de Juan, F. Non-abelian gauge fields and quadratic band touching in molecular graphene. *Phys. Rev. B* **87**, 125419 (2013).
- Sugawa, S., Salces-Carcoba, F., Perry, A. R., Yue, Y. & Spielman, I. Second Chern number of a quantum-simulated non-abelian Yang monopole. Science 360, 1429 (2018).
- 26. Ye, W. et al. Photonic hall effect and helical zitterbewegung in a synthetic weyl system. *Light*.: Sci. Appl. **8**, 49 (2019).
- Liu, X.-J., Law, K. T. & Ng, T. K. Realization of 2d spin-orbit interaction and exotic topological orders in cold atoms. *Phys. Rev. Lett.* 112, 086401 (2014).
- Wang, Z.-Y. et al. Realization of an ideal Weyl semimetal band in a quantum gas with 3d spin-orbit coupling. Science 372, 271 (2021).
- 29. Li, C.-H. et al. Bose-Einstein condensate on a synthetic topological Hall cylinder. *PRX Quantum* **3**, 010316 (2022).
- 30. Liang, Q. et al. Chiral dynamics of ultracold atoms under a tunable SU (2) synthetic gauge field. *Nat. Phys.* **20**, 1738 (2024).
- 31. Wu, J. et al. Non-abelian gauge fields in circuit systems. *Nat. Electron.* **5**, 635 (2022).
- 32. Qian, L., Zhang, W., Sun, H. & Zhang, X. Non-abelian topological bound states in the continuum. *Phys. Rev. Lett.* **132**, 046601 (2024).
- Cheng, D. et al. Non-abelian lattice gauge fields in photonic synthetic frequency dimensions. *Nature* 637, 52 (2025).
- 34. Yuan, L., Lin, Q., Xiao, M. & Fan, S. Synthetic dimension in photonics. *Optica* **5**, 1396 (2018).
- 35. Lustig, E. & Segev, M. Topological photonics in synthetic dimensions. *Adv. Opt. Photonics* **13**, 426 (2021).
- Ehrhardt, M., Weidemann, S., Maczewsky, L. J., Heinrich, M. & Szameit, A. A perspective on synthetic dimensions in photonics. *Laser Photonics Rev.* 17, 2200518 (2023).
- Hazzard, K. R. & Gadway, B. Synthetic dimensions. Phys. Today 76, 62 (2023).
- 38. Yu, D. et al. Comprehensive review of developments of synthetic dimensions. *Photonics Insights* **4**, R06 (2025).
- Armitage, N., Mele, E. & Vishwanath, A. Weyl and Dirac semimetals in three-dimensional solids. Rev. Mod. Phys. 90, 015001 (2018).
- 40. Bayer, M. et al. Optical modes in photonic molecules. *Phys. Rev. Lett.* **81**, 2582 (1998).
- 41. Zhang, M. et al. Electronically programmable photonic molecule. *Nat. Photonics* **13**, 36 (2019).
- Hafezi, M., Mittal, S., Fan, J., Migdall, A. & Taylor, J. Imaging topological edge states in silicon photonics. *Nat. Photonics* 7, 1001 (2013).
- Mittal, S., Ganeshan, S., Fan, J., Vaezi, A. & Hafezi, M. Measurement of topological invariants in a 2d photonic system. *Nat. Photonics* 10, 180 (2016).
- 44. Dutt, A. et al. A single photonic cavity with two independent physical synthetic dimensions. *Science* **367**, 59 (2020).
- 45. Cheng, D., Wang, K. & Fan, S. Artificial non-abelian lattice gauge fields for photons in the synthetic frequency dimension. *Phys. Rev. Lett.* **130**, 083601 (2023).
- 46. Li, G. et al. Direct extraction of topological Zak phase with the synthetic dimension. *Light.: Sci. Appl.* **12**, 81 (2023).
- Sridhar, S. K., Ghosh, S., Srinivasan, D., Miller, A. R. & Dutt, A. Quantized topological pumping in Floquetÿsynthetic dimensions with a driven dissipative photonic molecule. *Nat. Phys.* 20, 843–851 (2024).

- Pellerin, F., Houvenaghel, R., Coish, W., Carusotto, I. & St-Jean, P. Wave-function tomography of topological dimer chains with longrange couplings. *Phys. Rev. Lett.* 132, 183802 (2024).
- Englebert, N. et al. Bloch oscillations of coherently driven dissipative solitons in a synthetic dimension. Nat. Phys. 19, 1014 (2023).
- 50. Helgason, Ó. B. et al. Dissipative solitons in photonic molecules. *Nat. Photonics* **15**, 305 (2021).
- Hu, Y., Reimer, C., Shams-Ansari, A., Zhang, M. & Loncar, M. Realization of high-dimensional frequency crystals in electro-optic microcombs. *Optica* 7, 1189 (2020).
- 52. Balčytis, A. et al. Synthetic dimension band structures on a Si CMOS photonic platform. *Sci. Adv.* **8**, eabkO468 (2022).
- 53. Javid, U. A. et al. Chip-scale simulations in a quantum-correlated synthetic space. *Nat. Photonics* **17**, 883 (2023).
- 54. Dikopoltsev, A. et al. Topological insulator quantum cascade laser in synthetic space: towards a realization, in *European Quantum Electronics Conference* (Optica Publishing Group, 2023).
- 55. Bouhon, A. et al. Non-abelian reciprocal braiding of Weyl points and its manifestation in zrte. *Nat. Phys.* **16**, 1137 (2020).
- 56. Guo, Q. et al. Experimental observation of non-abelian topological charges and edge states. *Nature* **594**, 195 (2021).
- 57. Yang, Z. et al. Mode-locked topological insulator laser utilizing synthetic dimensions. *Phys. Rev. X* **10**, 011059 (2020).
- Dong, Z., Chen, X., Dutt, A., & Yuan, L. Topological dissipative photonics and topological insulator lasers in synthetic timefrequency dimensions. *Laser & Photonics Reviews*, 2300354 (2024).
- Barnett, R., Boyd, G. R. & Galitski, V. Su (3) spin-orbit coupling in systems of ultracold atoms. *Phys. Rev. Lett.* 109, 235308 (2012).

Acknowledgments

The research was supported by the National Key R&D Program of China (No. 2023YFA1407200), the National Natural Science Foundation of China (12122407 and 12192252).

Author contributions

Z.D. initiated the idea and performed the simulation. Z.D. and L.Y. discussed the results. Z.D. and L.Y. wrote the draft. Z.D., X.C., and L.Y. revised the manuscript. L.Y. supervised the project.

Competing interests

The authors declare no competing interests.

Additional information

Supplementary information The online version contains supplementary material available at https://doi.org/10.1038/s41467-025-65214-z.

Correspondence and requests for materials should be addressed to Luqi Yuan.

Peer review information: *Nature Communications* thanks Gui-Geng Liu, Yan-Qing Zhu, and the other, anonymous, reviewers for their contribution to the peer review of this work. A peer review file is available.

Reprints and permissions information is available at http://www.nature.com/reprints

Publisher's note Springer Nature remains neutral with regard to jurisdictional claims in published maps and institutional affiliations.

Open Access This article is licensed under a Creative Commons Attribution-NonCommercial-NoDerivatives 4.0 International License, which permits any non-commercial use, sharing, distribution and reproduction in any medium or format, as long as you give appropriate credit to the original author(s) and the source, provide a link to the Creative Commons licence, and indicate if you modified the licensed material. You do not have permission under this licence to share adapted material derived from this article or parts of it. The images or other third party material in this article are included in the article's Creative Commons licence, unless indicated otherwise in a credit line to the material. If material is not included in the article's Creative Commons licence and your intended use is not permitted by statutory regulation or exceeds the permitted use, you will need to obtain permission directly from the copyright holder. To view a copy of this licence, visit http://creativecommons.org/licenses/by-nc-nd/4.0/.

© The Author(s) 2025